Origin and nature of coke in ethanol steam reforming and its role in deactivation of Ni/La_2O_3-αAl_2O_3 catalyst

Carolina Montero[a], Aingeru Remiro[b], Beatriz Valle[b], Lide Oar-Arteta[b,c], Javier Bilbao[b], Ana G. Gayubo[b]*

[a] *Chemical Engineering Faculty, Central University of Ecuador, Ciudad Universitaria-Ritter s/n y Bolivia. Quito, Ecuador. Phone: +593 22544631. Fax: +593 22529676*

[b] *Chemical Engineering Department, University of the Basque Country, P.O. Box 644, 48080. Bilbao, Spain. Phone: +34 946 015361. Fax: +34 946 013 500*

[c] *Catalysis Engineering / ChemE / TUDelft, Van der Maasweg 9, 2629 HZ Delft (The Netherlands)*

*email: carodrmontero@gmail.com

Abstract

Deactivation of Ni/La_2O_3-αAl_2O_3 catalyst in the ethanol steam reforming (ESR) was studied in order to establish the optimal conditions for maximizing H_2 production and achieving a steady behaviour. The ESR reactions were conducted in a fluidized bed reactor under the following operating conditions: 500-650 ºC; space-time up to 0.35 $g_{catalyst}h/g_{EtOH}$; and steam/ethanol (S/E) molar ratio in the feed, 3-9. The features of the deactivated catalysts, and the nature and morphology of the coke deposited were analysed by Temperature Programmed Oxidation, X-Ray Diffraction, Scanning Electron Microscopy, and Raman Spectroscopy. Catalyst deactivation was solely caused by coke deposition, especially by encapsulating coke, with acetaldehyde, ethylene and ethanol being the main precursors, whose concentration was high for lower values of space-time. Conversely, the filamentous coke formed from CH_4 and CO (with their highest concentration for intermediate values of space-time) had a much lower impact on deactivation. Owing to the effect space-time has on the extent of reactions leading to the formation of coke precursors, the Ni/La_2O_3-αAl_2O_3 catalyst stability was enhanced by increasing space-time. The increase in temperature and S/E ratio was also beneficial, since both variables promoted coke gasification. Consequently, a steady H_2 yield throughout 200 h reaction was attained at 600 ºC, space-time of 0.35 $g_{catalyst}h/g_{EtOH}$ and S/E > 3.

Keywords: deactivation; coke; ethanol; hydrogen production; steam reforming; fluidized reactor

1. Introduction

Progress toward the development of efficient and environmentally friendly technologies for producing H_2 from biomass would reduce the CO_2 emissions coming from its current production process (i.e., reforming and partial oxidation of methane) [1]. Among alternative routes, the steam reforming (SR) of biomass derivatives is more advantageous in terms of production costs than thermal processes of pyrolysis and gasification [2].

The competitive advantage of steam reforming of bio-ethanol over other biomass derivatives (e.g., bio-oil, methanol, dimethyl ether) lies in its higher hydrogen content, in addition to its high reactivity at low temperature (300 ºC), non-toxicity, storage and handling ease, and safety. Furthermore, the large-scale production of bio-ethanol from lignocellulosic biomass by hydrolysis-fermentation has good prospects [3-7], and the SR of bio-ethanol (8-12 wt% water) would avoid the ethanol dehydration costs required for its use as a fuel [6]. Noble metal supported catalysts (especially Rh-based catalysts) have been reported as highly active and selective for ethanol steam reforming (ESR) [8-10]. However, Ni and Co based catalysts have been mostly studied due to their high C-C bond breakage activity and lower cost. These catalysts are conventionally synthesized by impregnating the metal oxide on different supports, such as Al_2O_3, SiO_2, CeO_2 or ZrO_2 [11-17]. Catalysts derived from perovskite type mixed oxides [18-21], spinel type catalysts [22-24], and those combining noble and non-noble metals have also been used [25, 26].

Ethanol steam reforming (ESR) is an endothermic process with the following ideal stoichiometry:

$$C_2H_5OH + 3\ H_2O \rightarrow 6\ H_2 + 2\ CO_2 \qquad \Delta H_{298}^{0} = 173.3\ \text{kJ/mol} \tag{1}$$

The actual H_2 yield is lower than the stoichiometric value, Eq. (1), owing to the formation of intermediate compounds and by-products through other side reactions, whose prevalence depend on the catalyst and operating conditions [4,5,27-29]. These side reactions include (Table 1): ethanol dehydrogenation and dehydration, decomposition of ethanol and acetaldehyde, and subsequent reactions of decomposition products (e.g., water gas shift reaction (WGS), CO methanation, steam reforming of methane and of ethylene).

Nevertheless, the reactions that have a more adverse impact on H_2 production are those leading to coke formation, which causes catalyst deactivation. These reactions (also gathered in Table 1) include: cracking of ethanol and acetaldehyde, ethylene polymerization, methane decomposition and Boudouard reaction. Attenuation of these reactions extent, which depends on the composition and properties of the catalyst and the reaction conditions, is a priority objective that needs to be addressed with a view to the economic feasibility of ESR. For this purpose, it must be taken into account that there is no linear relationship between the decrease in catalyst activity and the coke content. This fact is a consequence of the heterogeneous nature of the coke, composed of amorphous and filamentous fractions, with the coke of amorphous structure having a greater impact on deactivation due to encapsulation of the active metal sites [28,30-32].

Table 1

Different strategies aimed at selecting and modifying catalysts have been proposed in the literature for minimizing coke deposition over transition metal catalysts, which undergo greater deactivation than noble metal catalysts [4,6]. Such efforts include the use of bimetallic catalysts (such as Pt-Ni, Ru-Ni, Ru-Co, Cu-Ni, Ni-Co) [33], and modifications of the most commonly studied support Al_2O_3 by: i) doping with ZrO_2, Y_2O_3, CaO, MgO or La_2O_3 in order to passivate the acidity, thus minimizing ethylene formation and its subsequent polymerization to coke; and ii) adding materials with high oxygen storage ability (such as CeO_2 and La_2O_3) in order to promote oxidation of deposited carbon [34]. The use of perovskite, spinel, and hydrotalcite (HT)-derived mixed oxides as catalysts and supports has proved to stabilize highly dispersed metal nanoparticles, thus decreasing coke deposition. It has also been reported that Ni-encapsulated graphene chainmail catalyst (with a core-shell structure) improves the stability of conventional Ni supported catalysts by avoiding sintering and oxidation of Ni [35].

The scheme of the reactions involved in ESR over the Ni/La_2O_3-αAl_2O_3 catalyst has been established in a previous work [36]. After a prior equilibration cycle, this catalyst recovers its activity in successive reaction-regeneration cycles [37]. The complexity of the deactivation dynamics was also previously proved, showing three different stages in the evolution with time on stream of product yields at 500 ºC [38]: i) Stage 1, ascribed to the formation of filamentous coke with little impact on the catalyst activity; ii) Stage 2, related to the formation of a more condensed and graphitic coke that causes severe deactivation by encapsulating the Ni sites; and iii) Stage 3, ascribed to slow deposition of a highly-deactivating amorphous coke which covers almost completely the catalyst surface. These previous results evidenced that the amount and nature of the coke, and its impact on the catalyst deactivation are greatly influenced by the reforming conditions.

Consequently, this work focuses on studying formation and evolution of coke in order to establish suitable operating conditions (temperature, S/E molar ratio and space-time) that minimize Ni/La_2O_3-αAl_2O_3 catalyst deactivation. For this purpose, special emphasis has been placed on identifying the coke precursors by relating the characteristics of the coke with the concentration of compounds in the reaction medium. ESR reactions have been carried out in a fluidized bed reactor, which has good perspectives for the scaling-up, enables thermal uniformity of the catalytic bed, and attenuates deactivation by coke deposition [39]. The deactivated catalyst samples have been collected after each reaction and characterized by Temperature Programmed Oxidation (TPO), X-Ray Diffraction (XRD), N_2 adsorption-desorption, Raman Spectroscopy and Scanning Electronic Microscopy (SEM). In order to properly ascertain the role of reaction medium compounds in the formation of coke, this study covers a wide range of reaction conditions to include: i) reactions with low conversion, and hence high concentration of ethanol and intermediate compounds; ii) reactions with high conversion (close to thermodynamic regime), and hence high concentration of final carbon by-products (CO and CH_4).

2. Experimental section

2.1. Catalyst synthesis and characterization

The Ni/La_2O_3-αAl_2O_3 catalyst (with 10 wt% Ni and 9 wt% La_2O_3 nominal contents) was prepared by incipient wetness impregnation, and calcined at 550 ºC for 2 h. Prior to its use in the ESR reactions, the catalyst was equilibrated in order to provide reproducible behavior in successive reaction cycles with intermediate regeneration by coke combustion [37]. The catalyst properties were reported elsewhere [36]: metal contents close to nominal values (8.8 % Ni and 6.8 % La, measured by ICP-AES); BET surface area of 35 m^2/g; Ni^0 metal surface area and dispersion of 3.1 m^2/g and 4.7 %, respectively; and Ni^o crystal size of 10.6 nm. Before each reaction, the catalyst was reduced *in situ* at 700 °C for 2 h by using a H_2–He flow (10 vol% H_2).

X-ray diffraction technique (XRD) was used to characterize the crystallinity and Ni^0 particle size (by applying the Debye-Scherrer approach at $2\theta = 52^o$) using a Philips X´PERT PRO diffractometer at 40 kV and 40 mA, in theta–theta configuration, with a secondary monochromator with Cu Ka1 radiation at a wavenumber of 1.5418 Å. The great amount of coke may hinder a proper detection of Ni diffraction peaks in deactivated catalyst samples. Therefore, XRD analyses were conducted after removing the coke deposited (by combustion with air at 500 ºC for 2 h) and subsequent reduction of NiO_x species formed during combustion (in H_2/N_2 stream at 700 ºC for 2 h). The BET surface and porous structure were analyzed by N_2 adsorption−desorption in a Quantacrome Autosorb IQ2 in physisorption mode.

The coke deposited was analyzed by: (i) TPO for qualitative characterization of the coke nature and quantitative determination of coke content. A Thermo Scientific TGA Q5000TA thermobalance connected on-line to a Thermostar (Balzers Instruments) mass spectrometer was used to record the CO_2 signal during combustion, which allowed quantification of coke content since thermogravimetric signal is masked by Ni oxidation. (ii) Raman spectroscopy for determining the crystallinity degree of the coke. These analyses were performed in a Renishaw InVia confocal microscope using an excitation wavelength value of 514 nm. (iii) SEM images for determining the morphology of the coke (encapsulating or filamentous). These images were obtained using a JEOL/JSM-7000F microscope, equipped with energy dispersive spectroscopy (EDS) accessories and operating at 25 kV.

2.2. Reaction equipment and experimental conditions

The automated reaction equipment (Microactivity reference-PID Eng & Tech) consisted of an isothermal fluidized bed reactor (22 mm internal diameter and 460 mm length), described elsewhere [40]. The reactor was connected on-line to a gas chromatograph (MicroGC Agilent 3000) provided with four modules for analysing the reaction products: 1) permanent gases (O_2, N_2, H_2, CO, and CH_4) with a 5A molecular sieve capillary column; 2) light oxygenates (C_{2-}), CO_2 and water with Plot Q capillary column; 3) C_2-C_4 hydrocarbons with alumina capillary column; 4) oxygenated compounds (C_{2+}) with Stabilwax type column. The compounds were identified and quantified with calibration standards of known concentration. The C, H, O mass balance closure was above 98 % for all the experiments.

The catalyst particles (0.15-0.25 mm) were mixed with inert solid (SiC, 37µm) in inert:catalyst mass ratio > 8:1 in order to have bed height/diameter ratio ≈ 2. The gas flow-rate and linear velocity at the reactor inlet was 7.6 cm^3/s and 2.4 cm/s, respectively (6 times the minimum fluidization velocity). These fluid-dynamic conditions were previously established for ensuring proper catalytic bed fluidization and avoiding internal and external diffusional restrictions within the catalyst particles [13].

The operating conditions for ESR reactions were: 500 - 650 °C range (the upper limit was set to avoid an excessive conversion of ethanol by thermal routes [36]); steam/ethanol molar ratio (S/E) between 3 and 9; space-time between 0.02 and 0.35 $g_{catalyst}h/g_{EtOH}$ (catalyst mass between 0.03 and 0.525 g); total pressure, 1.4 bar; and ethanol partial pressure, 0.083 bar. The duration of each reaction was 20 h, except for some long-term experiments (200 h).

The ethanol conversion (X) was calculated from its molar flow-rate (F) at the inlet and outlet of the reactor, according to the following equation:

$$X = \frac{F_{inlet} - F_{outlet}}{F_{inlet}} \tag{15}$$

The yield of each product (Y_i) was calculated as the ratio between its molar flow-rate (F_i) and the maximum molar flow-rate that can be obtained from, according to stoichiometry:

$$Y_i = \frac{F_i}{\upsilon_i \cdot F_{inlet}} \tag{16}$$

where $\upsilon_i = 6$ for H_2, $\upsilon_i = 2$ for CO_2, CO and CH_4, and $\upsilon_i = 1$ for acetaldehyde and ethylene. Other intermediate compounds were not detected in the operating condition range studied.

3. Results and discussion

The effect temperature, S/E ratio and space-time have on the evolution with time on stream of ethanol conversion and product yields is discussed in Section 3.1. Special attention has been paid on the composition of the reaction medium, and the relative prevalence of each coke formation reaction (Table 1) under the different operating conditions. The deactivation results will be related to the content and nature of the coke in Section 3.2 (cause and effect relationship). This will allow identifying the coke precursors, and establishing suitable operating conditions for minimizing deactivation (Section 4).

3.1. Effect of operating conditions on the catalyst stability

This section analyses the effect temperature, space-time and S/E molar ratio have on the evolution with time on stream of ethanol conversion and product yields (H_2, CO_2, CO, CH_4, acetaldehyde and ethylene) resulting from ethanol steam reforming and side reactions. The relationship between reactants and products of these reactions has been schematically described in a previous work [36].

3.1.1. Effect of temperature

Figures 1 and 2 show the evolution with time on stream (TOS) of ethanol conversion and product yields for different reaction temperatures. Each figure corresponds to a different value of space-time, which is useful for studying the catalyst deactivation in a reaction medium with different concentration of reactants and products. Figure 1 corresponds to a low space-time (0.02 $g_{catalyst}h/g_{EtOH}$), and thus to a low extent of reaction. At 500 °C (Figure 1a), the initial conversion of ethanol is very low and decreases rapidly, so that the major compounds in the reaction medium are ethanol and acetaldehyde (by-product formed by ethanol dehydrogenation). At 650 °C (Figure 1b), there is a rapid deactivation for 4 h TOS, and afterwards ethanol conversion reaches a steady value corresponding to the thermal pathways (catalyst is completely deactivated) [36]. Under these conditions, acetaldehyde is the major compound, and there is also a notable concentration of ethylene (formed by ethanol dehydration).

Figure 2 corresponds to a higher space-time (0.18 $g_{catalyst}h/g_{EtOH}$), and thus a greater extent of reaction. The initial conversion of ethanol (at zero TOS) is complete in the whole range of temperature (500-650 ºC), and it decreases after 12 h of reaction at 600 °C and after 5 h at 500 °C due to catalyst deactivation. The yield of each product evolves differently with TOS due to the complex effect of deactivation on each reaction of the kinetic scheme. Thus, the evolution with TOS of H_2 and CO_2 yields (Figures 2b and 2c, respectively) have the same trend, which is also similar to that of ethanol conversion, because they are final products of the SR and WGS reactions.

Nevertheless, carbon by-products show different trend (Figure 2) which can be explained by their different nature of primary, intermediate or final product within the reaction scheme. Thus, the CO yield increases slowly throughout reaction at 600 and 650 ºC, due to the selective catalyst deactivation for WGS and methanation reactions. The progressive increase in CH_4 yield at 650 ºC (Figure 2e) indicates that reforming of this by-product is also affected by deactivation. The maximum observed in the CO yield at 500 °C (Figure 2d) is due to the fact that acetaldehyde decomposition decreases after 10 h (Figure 2e). It should be noted that ethylene yield is significant for a low space-time (Figure 1) but negligible under the reaction conditions of Figure 2. The progressive decrease in CH_4 yield at 500 °C (Figure 2e) can be attributed to the catalyst deactivation for CO methanation. The afore-mentioned deactivation of acetaldehyde decomposition also contributes to the faster decrease observed in CH_4 yield after 10 h TOS. These trends are qualitatively similar to those observed for other S/E ratios (results not shown). It should be mentioned that these results are consistent with those reported in the literature for other catalysts [28,41], which reveal improvement of catalyst stability by increasing temperature in the range 500-650 ºC, under conditions of high ethanol conversion.

These results evidence that, regardless the operating conditions used, acetaldehyde concentration in the reaction medium is high during the period of rapid catalyst deactivation (from zero TOS in Figure 1 and from 10 h TOS in Figure 2). The role of this by-product as a coke precursor (Eq. 10) will be confirmed below. Furthermore, the role of ethanol as a coke precursor (by cracking, Eq. 9) or by condensation of ethyl oxonium ions into aromatic structures should not be discarded.

Figure 1

Figure 2

3.1.2. Effect of steam/ethanol (S/E) molar ratio

The effect of S/E molar ratio on the evolution with TOS of ethanol conversion and H_2 yield (Figure 3a), and yields of the main carbon by-products (CO and CH_4, Figure 3b) is analyzed in this section. The results correspond to 500 °C (for which deactivation is remarkable, as shown in Section 3.1.1) and space-time of 0.18 $g_{cat}h/g_{EtOH}$.

Figure 3

These results, consistent with those reported in the literature for other catalysts [6,28,42], show that the increase in S/E ratio favors the H_2 production by enhancing the extent of SR and WGS reactions. Besides, catalyst deactivation is notably attenuated, especially from 3 to 6, with this effect being less noticeable in the 6-9 range. Similar effect of S/E ratio on catalyst deactivation has been observed for other values of temperature and space-time (not shown).

3.1.3. Effect of space-time

The effect that space-time has on the deactivation dynamics is analyzed in Figure 4. This shows the evolution with TOS of ethanol conversion (a), and yields of H_2 (b), CO (c), CH_4 (d), acetaldehyde (e) and ethylene (f) at 550 °C for three values of space-time. The evolution with TOS of CO_2 yield (not shown) has a similar trend to that of H_2.

Figure 4

The rapid decrease in ethanol conversion and product yields at the lowest value of space-time (0.02 $g_{catalyst}h/g_{EtOH}$) evidences a very fast deactivation rate. Consequently, all products tend rapidly towards the yields corresponding to thermal routes [36], with acetaldehyde (Figure 4e) and ethylene (Figure 4f) being the only compounds when the catalyst is fully deactivated. The decrease in ethanol conversion and H_2 yield is attenuated by increasing space-time, with both parameters decreasing by only 5 % after 20 h reaction for 0.17 $g_{catalyst}h/g_{EtOH}$. The absence of acetaldehyde and ethylene for values above 0.17 $g_{catalyst}h/g_{EtOH}$ is a consequence of the total extent of their transformation reactions (by decomposition and steam reforming, respectively).

The rapid deactivation observed under conditions with high yields of intermediate products (acetaldehyde and ethylene) and reactant (ethanol) reveals the significant role of these compounds in the catalyst deactivation (Eqs 9-11). Conversely, CO and CH_4 by-products have little contribution, as suggested by their low concentration in the reaction medium under conditions of rapid deactivation.

Furthermore, two steam reforming reactions were carried out with pure acetaldehyde (ASR reactions) in order to verify the role that this compound has in Ni/La_2O_3-αAl_2O_3 catalyst deactivation (Eq 11). The operating conditions were: 600 ºC, steam-to-acetaldehyde (S/Ac) molar ratio of 12.3, space-time of 0.04 and 0.21 $g_{catalyst}h/Ac$, partial pressure of 0.083 bar. The results (Figure S1 of Supporting Information) confirm a very fast catalyst deactivation when acetaldehyde concentration in the reaction medium is high (Figure S1a, corresponding to low space-time and low conversion), which is notably attenuated when the concentration of acetaldehyde is lower (Figure S1b, corresponding to high space-time and high conversion).

3.2. Analysis of deactivated catalyst

It is a well-known fact that coke deposition and metal sintering are the major causes of Ni-based catalysts deactivation in the ESR. The deterioration of porous structure and metal surface properties of Ni/La_2O_3-αAl_2O_3 catalyst is analyzed in Section 3.2.1 in order to ascertain the significance of Ni sintering under the studied conditions. In section 3.2.2, content and nature of the coke is studied and related to the deactivation observed in Section 3.1.

3.2.1. Catalyst surface deterioration

Deactivated catalyst samples have been analyzed by adsorption-desorption of N_2 (as described in Section 2.1) to determine any deterioration of the porous structure. The results of S_{BET}, pore volume and average pore size (Table 2) reveal the importance of space-time. For a low space-time (0.04 $g_{catalyst}h/g_{EtOH}$), physical properties of deactivated catalyst are very similar to those of the fresh catalyst, and hence aging of the support and pores blocking by coke can be discarded as causes of catalyst deactivation. However, for a high space-time (0.18 $g_{catalyst}h/g_{EtOH}$), the S_{BET} of deactivated catalyst is markedly higher (156.6 m^2 g^{-1}) than that of the fresh one (35.3 m^2 g^{-1}), and volume and size of pores are noticeably lower. The influence that space-time has on the catalyst porous structure can be attributed to different amount and morphology of the coke deposited, as described in Section 3.2.2.

Table 2

The possible Ni sintering has been studied on the basis of Ni^0 crystal size of the catalysts used in long-term experiments (200 h) at 600 and 650 ºC, determined by XRD diffractometry (by means of Scherrer equation at $2\theta = 52$ º). The results (Table 3) do not show a significant increase in crystal size, even for the most severe conditions (650 ºC and S/E = 6) for which the size is similar to that of the fresh catalyst (10.6 nm). This fact reveals the insignificant role of Ni sintering, which is consistent with the evolution with TOS of ethanol conversion and product yields during the long-term experiments conducted at high temperature (shown below).

Table 3

3.2.2. Content and nature of the coke

The effect space-time has on the TPO results of the coke deposited at 500 ºC (Graph a), and 600 ºC (Graph b) is shown in Figure 5. The corresponding results of total coke content are shown in Figure 6. All the TPO profiles show a single peak whose intensity and combustion temperature significantly depends on space-time, thus revealing the notable effect of this variable on the nature of the coke deposited. For low values of space-time (≤ 0.04 $g_{catalyst}h/g_{EtOH}$) the combustion peak is located below 400 ºC, whereas for space-time ≥ 0.09 $g_{catalyst}h/g_{EtOH}$ (and consequently, higher extent of reaction) there is a wider peak located above 550 ºC.

Figure 5

Figure 6

Based on the available literature on TPO of catalysts used in ESR reaction, formation of different types of coke has been reported depending on the catalyst and reaction conditions used [28,30,43,44]. Overall, combustion peaks at low temperatures (< 450 ºC) have been ascribed to amorphous coke deposited on the metal, which catalyzes its rapid combustion, whereas combustion peaks at higher temperatures correspond to a coke with fibrillar structure and different graphitization degree (including carbon filaments), which is located far from the metal [38]. The coke deposited on the metal sites (encapsulating) causes a rapid deactivation, whereas the filamentous coke has less incidence in catalyst deactivation, since it does not block the active metal sites [28].

The total amount of coke is also greatly affected by the space-time used, showing a maximum coke content at intermediate values for different temperatures and S/E ratios (Figure 6). At 500 ºC (Figure 6a), the maximum coke deposition is shifted to higher space-time values as S/E ratio is increased, but it is not affected at 650 ºC (Figure 6b). These results evidence different content and nature of the coke, consequence of the effect that space-time has on the concentration of coke precursors. The mechanism of coke formation will be different depending on these precursors, as explained below.

The effect reforming temperature has on the TPO results of the coke deposited for a low value of space-time (Graph a) and intermediate value (Graph b) is shown in Figure 7. The results for S/E ratios other than 6 are qualitatively similar. The effect of reforming temperature is also noticeable, although it is less significant than the effect of space-time. All the samples show a single asymmetric combustion peak, with its maximum located in the 350-430 ºC range for the lowest space-time, and in 560-660 ºC for higher space-time, in agreement with the combustion peaks observed in Figure 5. Both peaks shift towards higher combustion temperature as reaction temperature is raised, which reveals a more condensed and graphitic nature of the coke, with lower H/C ratio and more difficult to burn [38,45-47].

Figure 7

These results also suggest that the effect reforming temperature has on the total amount of coke deposited depends on the space-time used. Thus, for a very low space-time (0.02 $g_{catalyst}h/g_{EtOH}$, Figure 7a) there is almost negligible coke content which increases moderately with temperature (from 0.7 wt% at 500 °C to 1.8 wt% at 650 °C). However, for intermediate space-time (0.09 $g_{catalyst}h/g_{EtOH}$, Figure 7b) the coke content at 500 °C is very high (60 wt %) and it decreases markedly as temperature is raised (to 2.3 wt % at 650 °C). This different trend ratifies the hypothesis of the different mechanism of coke formation that exists when the extent of the reforming reaction is low or high.

The effect S/E ratio has on the TPO results is shown in Figure 8. This figure corresponds to an intermediate value of space-time (0.18 $g_{catalyst}h/g_{EtOH}$) and two temperatures, 500 ºC (Figure 8a) and 600 ºC (Figure 8b). After reforming at 500 ºC (Figure 8a), combustion temperature of the coke (~580 ºC) does not vary significantly with S/E ratio, whereas at 600 ºC (Figure 8b) the combustion peak slightly shifts towards lower temperatures as S/E ratio is raised (625, 623 and 616 ºC, for S/E of 3, 6 and 9, respectively). This result is explained by a slightly more hydrogenated nature of the coke when the water content in the reaction medium is higher. Nonetheless, the amount of coke deposited decreases noticeably by increasing S/E ratio at both temperatures, which is explained by: i) the attenuation of reactions that lead to the formation of coke precursors, and ii) the intensification of coke gasification (Eq 13), especially at high temperature [25]. Based on the results in Figure 8, the prevailing effect at 500 °C (Figure 8b) is presumably the first one (considering the low reaction temperature), whereas the notable effect of S/E at 600 °C can be attributed to the gasification of coke (in a state of incipient formation).

Figure 8

3.2.3. Morphology and structure of the coke

SEM and Raman spectroscopic techniques (described in Section 2.1) have been used to complement the TPO information of the coke deposited on deactivated catalysts. The TPO results obtained for different space-time values have been explained by possible differences in the nature (amorphous or filamentous coke) and structure of the coke (with different condensation degree). Figure 9 compares the morphology of the coke (SEM images) deposited for low (0.04 $g_{catalyst}h/g_{EtOH}$) and high (0.18 $g_{catalyst}h/g_{EtOH}$) space-time at 500 ºC and S/E = 6. Carbon filaments are clearly discerned in the catalyst deactivated for the highest space-time (Figure 9b), but they are not detected for the lowest value (Figure 9a). These images confirm the different nature of the coke and support the hypothesis that coke formation mechanism is conditioned by the composition of the reaction medium.

Figure 9

Raman spectroscopy is a suitable technique for analyzing amorphous carbonaceous materials which is useful for corroborating the different coke structures. Figure 10a shows the Raman results corresponding to the coke deposited at low space-time (0.04 $g_{catalyst}h/g_{EtOH}$), S/E = 3, and two different temperatures (550 ºC and 650 ºC). Figure 10b corresponds to high space-time (0.35 $g_{catalyst}h/g_{EtOH}$), 500 ºC, and two different values of S/E ratio. The Raman spectra have been deconvoluted into 4 characteristic lorentzian bands of coke [45,48,49]: i) G band (1580-1600 cm^{-1}) corresponding to ordered aromatic structures or graphitic structures; ii) D band (1350 cm^{-1}) ascribed to disordered aromatic structures that indicates the presence of unstructured carbons, multilayer nanotubes or microcrystalline graphite; iii) the band assigned to amorphous coke in turbostratic fashion due to bond vibrations close to the edges in highly disordered graphitic layers (1450-1510 cm^{-1}); and iv) the band assigned to sp^2-sp^3 bond vibrations in disordered graphitic layers, with aliphatic chains (~1200 cm^{-1}). Table 4 shows the results of the intensity ratio of D and G bands (I_D/I_G), and the location and width of the G band.

Figure 10

Table 4

Figure 10 and Table 4 evidence significant differences in the structure of the coke deposited for low and high space-time values, whereas the effect of temperature and S/E ratio on coke structure is less significant. Thus, for a high space-time, both D and G bands are narrower, the G band position is higher, and the I_D/I_G ratio is noticeably lower, which suggests a greater structuring degree of the coke [46]. As reforming temperature is raised, the I_D/I_G ratio decreases slightly, the G band is narrower and it is located at a higher Raman displacement value, thus indicating formation of more crystal structures. Although position and width of the G-band are very little affected by S/E ratio, the coke deposited for higher S/E has a greater crystallinity, as suggested by the lower I_D/I_G.

4. Discussion on precursors of coke formation

Based on the afore-mentioned results, the Ni/La_2O_3-αAl_2O_3 catalyst deactivation in the range of operating conditions used is caused by coke deposition. The relationship between the product yields (Section 3.1) and the content and nature of the coke (Section 3.2.2) points that the different deactivation rate can be attributed to the amount, location and morphology of the coke, which in turn depends on the reaction medium composition (concentration of each coke precursor).

4.1. Effect of reaction conditions on the formation and characteristics of coke

TPO results shown in Section 3.2.2 (Figures 5, 7 and 8) evidence that location and nature of the coke deposited in the 500-650 ºC range significantly depend on space-time, whereas temperature and S/E ratio have much lower effect. Thus, for low space-time values (≤ 0.04 $g_{catalyst}h/g_{EtOH}$) there is a low deposition of an encapsulating coke (Figure 7a) in the whole range of temperature and S/E studied. This result is consistent with the fast deactivation rate observed (Figure 1) despite the low amount of coke deposited in these conditions. However, a slight increase in space-time above 0.04 $g_{catalyst}h/g_{EtOH}$ entails a sharp increase in coke deposition, and for space-time ≥ 0.09 $g_{catalyst}h/g_{EtOH}$ there is a huge amount of a filamentous coke (Figures 7b and 8). Owing to location (far form the metal sites) and filamentous morphology of this coke (as evidenced by SEM, Figure 9), it has much lower impact on catalyst deactivation than the encapsulating coke. This fact explains the lower deactivation rate observed (Figures 2 and 4) despite the high amount of coke deposited (Figure 6).

Although temperature and S/E ratio do not affect the type of coke deposited, its amount and to a lesser extent its structure, are affected by both variables. On the one hand, the effect temperature has on the amount of coke deposited depends on the space-time used. Thus, for low values of space-time, the increasing temperature entails a slightly higher deposition of encapsulating coke which explains the slightly faster deactivation at 650 ºC (Figure 1b) than at 500 ºC (Figure 1a). For intermediate values of space-time, there is a great formation of filamentous coke, whose deposition decreases noticeably by increasing temperature (mainly in the 500-550 ºC range) which explains the attenuation in deactivation rate (Figure 2). On the other hand, the attenuation of catalyst deactivation observed as S/E ratio is increased (Figure 3) is explained by the lower amount of coke (Figure 8). Nevertheless, the coke combustion peak hardly varies with S/E ratio (especially for low temperature, Figure 8a), which evidences that S/E has a much lower impact on the coke structure than reforming temperature.

Raman spectra (Figure 10 and Table 4) are consistent with TPO results (Figures 5, 7 and 8) and SEM images (Figure 9). The Raman results reveal a more structured coke deposited for high space-time value compared with that deposited for low space-time. This is consistent with the fibrillar morphology of the former (Figure 9b) and non-fibrillar of the latter (Figure 9a), and also consistent with the respective high and low combustion temperature in the TPO profiles. Similarly, the higher crystallinity of the coke deposited at higher reforming temperature (deduced from Raman spectra) is consistent with the shift towards higher combustion temperature observed in TPO (Figure 7). Likewise, the higher crystallinity of the coke deposited for higher S/E ratios at low temperature is consistent with the symmetrical combustion peak observed in Figure 8a (that is, lower amount of coke burning at low temperature).

The content and morphology of the coke explain the differences in the porous structure of the catalyst deactivated in conditions of low and high space-time (Table 2). Accordingly, the porous structure is not appreciably changed by the low content of encapsulating coke (3.5 wt %) deposited for low space-time. However, the specific surface is significantly increased by the great amount of coke (60 wt %) deposited for high space-time, due to the filamentous nature and porous structure of this type of coke [28,30,38]. The decrease in pore size could be caused by a partial blockage of the support porous structure, due to the large number of coke filaments.

4.2. Precursors and mechanisms of coke formation

As indicated above, content and characteristics of the coke deposited at different reaction conditions can be explained by the concentration of compounds that are precursors in the formation of each type of coke (Table 1, Eqs 9-13). These compounds and the coke formation mechanisms have been identified by comparing the composition of the reaction medium (Figures 1-4) with the corresponding TPO results of the coke deposited (Figures 5, 7 and 8) at each operating condition. Thus, for a low space-time and low extent of SR reaction (Figure 1) there is a remarkable concentration of acetaldehyde and ethylene, whose formation is promoted by increasing temperature. Coke formation capability of these compounds by cracking and polymerization towards aromatics (Eqs. 10 and 11) is well established in the literature [50,51]. Therefore, acetaldehyde and ethylene are considered main precursors of the coke deposited for low space-time. Ethanol cracking (Eq 9) and formation of aromatics on the catalyst surface cannot be discarded, due to the reactivity of ethoxy ions (enhanced with temperature) whose concentration is high when there is a high concentration of ethanol. The greater concentration of acetaldehyde and ethylene with increasing reaction temperature explains the greater deposition of amorphous and encapsulating coke, resulting in higher deactivation rate (Figure 1).

Conversely, the great extent of ethanol and ethylene reforming reactions (Eqs 1 and 8) and acetaldehyde decomposition (Eq 4) for higher space-time (≥ 0.09 $g_{catalyst}h/g_{EtOH}$) results in high yields of CH_4 and CO (Figures 2 and 3) and very low yields of acetaldehyde and ethylene. Therefore, the precursors of filamentous coke formation under these conditions are CH_4 (by decomposition reaction, Eq 12), and CO (by Boudouard reaction, Eq 13). This origin of the filamentous coke explains the maximum coke content obtained for an intermediate value of space-time (Figure 6), since the yields of CH_4 and CO are maximum (Figure 4). Further increase in space-time enhances both CH_4 reforming and WGS reaction, which promotes the formation of CO_2, thus disfavoring the coke formation by Boudouard reaction. Likewise, the significant attenuation of coke deposition by increasing S/E ratio for any temperature and space-time (Figure 8) is explained by the decreasing concentration of coke precursors, and by promotion of coke gasification (Eq 14) especially at high temperature.

These findings about the precursors of different types of coke have been corroborated by the $Ni/La_2O_3\text{-}\alpha Al_2O_3$ deactivation results and the analysis of the coke deposited in the SR reaction of pure acetaldehyde. The experiments have been conducted with two values of space-time in order to have different concentration of coke precursors (acetaldehyde, CO and CH_4) in the reaction medium. The evolution with TOS of conversion and product yields is shown in Figure S1 (Supporting Information) and the corresponding TPO profiles of deactivated catalyst are shown in Figure S2. The TPO profile of the catalyst deactivated under a reaction medium with high concentration of acetaldehyde (low space-time, 0.04 $g_{cat}h/g_{Ac}$), shows a single combustion peak at 385 °C, which is ascribed to encapsulating coke deposited on the metal. The TPO of the catalyst deactivated in a reaction medium with very low concentration of acetaldehyde and high of CO and CH_4 (high space-time, 0.21$g_{cat}h/g_{Ac}$) shows a combustion peak at 602 °C which corresponds to a filamentous and graphitic coke.

It should be highlighted that the results of this work are interesting in view of the ESR scale-up, since they demonstrate that $Ni/Al_2O_3\text{-}aAl_2O_3$ catalyst deactivation is significantly attenuated by increasing space-time and temperature (especially in 500-600 ºC range). Therefore, it is possible to keep steady conversion and product yields during long-term operation at 600 ºC and a space-time of 0.35 $g_{catalyst}h/g_{EtOH}$, even under conditions of low S/E ratio in the feed (Figure 11, S/E = 3 stoichiometric ratio). As observed, a steady H_2 yield of around 65% is achieved throughout the whole reaction (200 h).

Figure 11

Considering the remarkable attenuation of $Ni/Al_2O_3\text{-}aAl_2O_3$ catalyst deactivation by increasing S/E ratio (especially in the 3-6 range), the steady period of ESR is likely to last longer by increasing this variable up to 6. The stability of this catalyst, already reported under certain conditions [36], has been confirmed by the afore-mentioned results on the dynamics of coke formation in a wide range of reaction conditions.

5. Conclusions

Ni/La_2O_3-αAl_2O_3 catalyst deactivation during the ESR in the 500-650 ºC range is only due to coke deposition because Ni sintering is negligible, even under the most severe reaction conditions. However, key factors in the deactivation are the nature and morphology of the coke, which depend mainly on the composition of the reaction medium. For a low space-time, acetaldehyde and ethylene (formed by dehydrogenation and dehydration of ethanol), as well as non-reacted ethanol, are the main precursors of coke formation. For a high space-time, the coke precursors are CH_4 and CO byproducts. Although temperature and S/E ratio affect the extent of reactions that lead to coke formation, and its condensation and gasification reactions, they play a secondary role in the nature and morphology of the coke,

The rapid catalyst deactivation for a low space-time is caused by deposition of encapsulating coke on the metal sites, which is formed by acetaldehyde and ethanol cracking and ethylene polymerization. The content of this type of coke is very low and it increases slightly with temperature. As space-time is raised, catalyst deactivation is attenuated owing to changes in the coke formation mechanism, with CH_4 (by decomposition) and CO (by Boudoard reaction) being the main precursors of a filamentous and partially graphitic coke. A further increase in space-time attenuates the deposition of this filamentous coke by decreasing CH_4 and CO concentration.

The increase in reaction temperature and S/E ratio has a significant contribution to attenuating catalyst deactivation by diminishing the concentration of coke precursors and enhancing coke gasification (especially at high temperature). Consequently, the greatest stability of the Ni/La_2O_3-αAl_2O_3 catalyst is achieved using the highest values of the three operating variables studied in this work. Thus, a steady H_2 production throughout 200 h reaction was attained at 600-650 ºC, with S/E ratio above 3 and space-time above 0.35 $g_{catalyst}g/g_{EtOH}$.

ACKNOWLEDGMENTS

This work has been carried out with financial support from the Ministry of Science and Technology of the Spanish Government and the ERDF Funds (Projects CTQ2012-35263 and CTQ2015-68883-R), the University of the Basque Country (UFI 11/39) and the Basque Government (Project IT748-13).

References

[1] A. Arregi, M. Amutio, G. Lopez, J. Bilbao, M. Olazar, Evaluation of thermochemical routes for hydrogen production from biomass: A review, Energy Convers. Manag. 165 (2018) 696–19. https://doi.org/10.1016/j.enconman.2018.03.089

[2] L. Kaiwen, Y. Bin, Z. Tao, Economic analysis of hydrogen production from steam reforming process: A literature review, Energ. Source. 13 (2018) 109–115. https://doi.org/10.1080/15567249.2017.1387619

[3] A. Hedayati, O. Le Corre, B. Lacarrière, J. Llorca, Dynamic simulation of pure hydrogen production via ethanol steam reforming in a catalytic membrane reactor, Energy 117 (2016) 316-324. https://doi.org/10.1016/j.energy.2016.06.042

[4] L.V. Mattos, G. Jacobs, B.H. Davis, F.B. Noronha, Production of hydrogen from ethanol: Review of reaction mechanism and catalyst deactivation, Chem. Rev. 112 (2012) 4094–4123. https://doi.org/10.1021/cr2000114

[5] T. Hou, S. Zhang, Y. Chen, D. Wang, W. Cai, Hydrogen production from ethanol reforming: Catalysts and reaction mechanism, Renew. Sust. Energy Rev. 44 (2015) 132-148. https://doi.org/10.1016/j.rser.2014.12.023

[6] Y.C. Sharma, A. Kumar, R. Prasad, S.N. Upadhyay, Ethanol steam reforming for hydrogen production: Latest and effective catalyst modification strategies to minimize carbonaceous deactivation, Renew. Sust. Energy Rev. 74 (2017), 89–103. https://doi.org/10.1016/j.rser.2017.02.049

[7] H.B. Aditiya, T.M.I. Mahlia, W.T. Chong, H. Nur, A.H. Sebayang, Second generation bioethanol production: A critical review, Renew. Sust. Energy Rev. 66 (2016) 631–653. https://doi.org/10.1016/j.rser.2016.07.015

[8] F. Wang, W. Cai, H. Provendier, Y. Schuurman, C. Descorme, C. Mirodatos, W. Shen, Hydrogen production from ethanol steam reforming over Ir/CeO_2 catalysts: Enhanced stability by PrO_x promotion, Int. J. Hydrogen Energy 36 (2011) 13566–13574. https://doi.org/10.1016/j.ijhydene.2011.07.091

[9] P. Osorio-Vargas, C.H. Campos, R.M. Navarro, J.L.G. Fierro, P. Reyes, Improved ethanol steam reforming on Rh/Al_2O_3 catalysts doped with CeO_2 or/and La_2O_3: Influence in reaction pathways including coke formation, Appl. Catal. A 505 (2015) 159-172. https://doi.org/10.1016/j.apcata.2015.07.037

[10] P.K. Sharma, N. Saxena, P.K. Roy, A. Bhatt, Hydrogen generation by ethanol steam reforming over Rh/Al_2O_3 and Rh/$CeZrO_2$ catalysts: A comparative study, Int. J. Hydrogen Energy 41 (2016) 6123-6133. https://doi.org/10.1016/j.ijhydene.2015.09.137

[11] A.F. Lucredio, J.D.A. Bellido, A. Zawadzki, E.M. Assaf, Co catalysts supported on SiO_2 and γ-Al_2O_3 applied to ethanol steam reforming: Effect of the solvent used in the catalyst preparation method, Fuel 90 (2011) 1424–1430. https://doi.org/10.1016/j.fuel.2010.12.036

[12] R. Trane-Restrup, S. Dahl, A.D. Jensen, Steam reforming of ethanol: Effects of support and additives on Ni-based catalysts, Int. J. Hydrogen Energy 38 (2013) 15105–15118. https://doi.org/10.1016/j.ijhydene.2013.09.027

[13] A.G. Gayubo., J. Vicente, J. Ereña, C. Montero, M. Olazar, J. Bilbao, Comparison of Ni and Co catalysts for ethanol steam reforming in a fluidized bed reactor, Catal. Lett. 144 (2014) 1134–1143. https://doi.org/10.1007/s10562-014-1265-x

[14] S.J. Han, J.H. Song, Y. Bang, J. Yoo, S. Park, K.H. Kang, I.K. Song, Hydrogen production by steam reforming of ethanol over mesoporous Cu-Ni-Al_2O_3-ZrO_2 xerogel catalysts, Int. J. Hydrogen Energy 41 (2016) 2554–2563. https://doi.org/10.1016/j.ijhydene.2015.11.128

[15] X. Zhao, G. Lu, Modulating and controlling active species dispersion over Ni-Co bimetallic catalysts for enhancement of hydrogen production of ethanol steam reforming, Int. J. Hydrogen Energy 41 (2016) 3349-3362. https://doi.org/10.1016/j.ijhydene.2015.09.063

[16] A.J. Vizcaino, A. Carrero, J.A. Calles, Comparison of ethanol steam reforming using Co and Ni catalysts supported on SBA-15 modified by Ca and Mg, Fuel Process. Technol. 146 (2016) 99–109. https://doi.org/10.1016/j.fuproc.2016.02.020

[17] A.D. Shejale, G.D. Yadav, Cu promoted Ni-Co/hydrotalcite catalyst for improved hydrogen production in comparison with several modified Ni-based catalysts via steam reforming of ethanol, Int. J. Hydrogen Energy 42 (2017) 11321–11332. https://doi.org/10.1016/j.ijhydene.2017.03.052

[18] K.-H. Lin, C.-B. Wang, S.-H. Chien, Catalytic performance of steam reforming of ethanol at low temperature over $LaNiO_3$ perovskite, Int. J. Hydrogen Energy 38 (2013) 3226–3232. https://doi.org/10.1016/j.ijhydene.2013.01.005

[19] L. Zhao, T. Han, H. Wang, L. Zhang, Y. Liu, Ni-Co alloy catalyst from $LaNi_{1-x}Co_xO_3$ perovskite supported on zirconia for steam reforming of ethanol, Appl. Catal. B 187 (2016) 19–29. doi.org/10.1016/j.apcatb.2016.01.007

[20] J. Shao, G. Zeng, Y. Li, Effect of Zn substitution to a $LaNiO_{3-\delta}$ perovskite structured catalyst in ethanol steam reforming, Int. J. Hydrogen Energy 42 (2017) 17362–17375. https://doi.org/10.1016/j.ijhydene.2017.04.066

[21] F.N. Agüero, J.A. Alonso, M.T. Fernández-Díaz, L.E. Cadus, Ni-based catalysts obtained from perovskites oxides for ethanol steam reforming, J. Fuel Chem. Technol. 46 (2018) 1332–1341. https://doi.org/10.1016/S1872-5813(18)30053-7

[22] F. Aupretre, C. Descorme, D. Duprez, D. Casanave, D. Uzio, Ethanol steam reforming over $Mg_xNi_{1-x}Al_2O_3$ spinel oxide-supported Rh catalysts, J. Catal. 233 (2005) 464–477. https://doi.org/10.1016/j.jcat.2005.05.007

[23] A. Olivares, M. Gomez, M. Barroso, M. Abell, Ni-supported catalysts for ethanol steam reforming: effect of the solvent and metallic precursor in catalyst preparation, Int. J. Ind. Chem. 9 (2018) 61–73. https://doi.org/10.1007/s40090-018-0135-6

[24] G.P. Szijjártó, Z. Pászti, I. Sajó, A. Erdohelyi, G. Radnóczi, A. Tompos, Nature of the active sites in Ni/$MgAl_2O_4$-based catalysts designed for steam reforming of ethanol, J. Catal. 305 (2013) 290–306. https://doi.org/10.1016/j.jcat.2013.05.036

[25] J.Y.Z. Chiou, C.L. Lai, S.-W. Yu, H.-H. Huang, C.-L. Chuang, C.-B. Wang, Effect of Co, Fe and Rh addition on coke deposition over Ni/$Ce_{0.5}Zr_{0.5}O_2$ catalysts for steam reforming of ethanol, Int. J. Hydrogen Energy 39 (2014) 20689–20699. https://doi.org/10.1016/j.ijhydene.2014.07.141

[26] T. Mondal, K.K. Pant, A.K. Dalai, Oxidative and non-oxidative steam reforming of crude bio-ethanol for hydrogen production over Rh promoted Ni/CeO_2-ZrO_2 catalyst, Appl. Catal. A 499 (2015) 19–31. https://doi.org/10.1016/j.apcata.2015.04.004

[27] M. Ni, D.Y.C. Leung, M.K.H. Leung, A review on reforming bio-ethanol for hydrogen production, Int. J. Hydrogen Energy 32 (2007) 3238-3247. https://doi.org/10.1016/j.ijhydene.2007.04.038

[28] J. Vicente, J. Ereña, C. Montero, M.J. Azkoiti, J. Bilbao, A.G. Gayubo, Reaction pathway for ethanol steam reforming on a Ni/SiO_2 catalyst including coke formation, Int. J. Hydrogen Energy 39 (2014) 18820-18834. https://doi.org/10.1016/j.ijhydene.2014.09.073

[29] C. Montero, L. Oar-Arteta, A. Remiro, A. Arandia, J. Bilbao, A.G. Gayubo, Thermodynamic comparison between bio-oil and ethanol steam reforming, Int. J. Hydrogen Energy 40 (2015) 15963-15971. https://doi.org/10.1016/j.ijhydene.2015.09.125

[30] J. Vicente, C. Montero, J. Ereña, M.J. Azkoiti, J. Bilbao, A.G. Gayubo, Coke deactivation of Ni and Co catalysts in ethanol steam reforming at mild temperatures in a fluidized bed reactor, Int. J. Hydrogen Energy 39 (2014) 12586–12596. https://doi.org/10.1016/j.ijhydene.2014.06.093

[31] B. Valle, B. Aramburu, P.L. Benito, J. Bilbao, A.G. Gayubo, Biomass to hydrogen-rich gas via steam reforming of raw bio-oil over Ni/La_2O_3-αAl_2O_3 catalyst: Effect of space-time and steam-to-carbon ratio, Fuel 216 (2018) 445–455. https://doi.org/10.1016/j.fuel.2017.11.151

[32] A. Ochoa, B. Valle, D.E. Resasco, J. Bilbao, A.G. Gayubo, P. Castaño, Temperature programmed oxidation coupled with in situ techniques reveal the nature and location of coke deposited on a Ni/La_2O_3-αAl_2O_3 catalyst in the steam reforming of bio-oil, ChemCatChem 10 (2018) 2311-2321. https://doi.org/10.1002/cctc.201701942

[33] C. Ruocco, V. Palma, A. Ricca, Experimental and kinetic study of oxidative steam reforming of ethanol over fresh and spent bimetallic catalysts, Chem. Eng. J. (2019) in press. https://doi.org/10.1016/j.cej.2018.08.164

[34] M. Chen, C. Wang, Y. Wang, Z. Tang, Z. Yang, H. Zhang, J. Wang, Hydrogen production from ethanol steam reforming: Effect of Ce content on catalytic performance of Co/Sepiolite catalyst, Fuel 247 (2019) 344–355. https://doi.org/10.1016/j.fuel.2019.03.059

[35] D. Chen, W. Wang, C. Liu, Ni-encapsulated graphene chainmail catalyst for ethanol steam reforming, Int. J. Hydrogen Energy 44 (2019) 6560–6572. https://doi.org/10.1016/j.ijhydene.2019.01.204

[36] C. Montero, A. Remiro, P.L. Benito, J. Bilbao, A.G. Gayubo, Optimum operating conditions in ethanol steam reforming over a Ni/La_2O_3-αAl_2O_3 catalyst in a fluidized bed reactor, Fuel Process. Technol. 169 (2018) 207–216. https://doi.org/10.1016/j.fuproc.2017.10.003

[37] C. Montero, A. Remiro, A. Arandia, P.L. Benito, J. Bilbao, A.G. Gayubo, Reproducible performance of a Ni/La_2O_3-αAl_2O_3 catalyst in ethanol steam reforming under reaction-regeneration cycles, Fuel Process. Technol. 152 (2016) 215–222. https://doi.org/10.1016/j.fuproc.2016.07.002

[38] C. Montero, A. Ochoa, P. Castaño, J. Bilbao, A.G. Gayubo, Monitoring Ni^0 and coke evolution during the deactivation of a Ni/La_2O_3–αAl_2O_3 catalyst in ethanol steam reforming in a fluidized bed, J. Catal. 331 (2015) 181-192. https://doi.org/10.1016/j.jcat.2015.08.005

[39] V. Palma, C. Ruocco, E. Meloni, A. Ricca, Oxidative reforming of ethanol over CeO_2-SiO_2 based catalysts in a fluidized bed reactor, Chem. Eng. Process. Process. Intensif. 124 (2018) 319-327. https://doi.org/10.1016/j.cep.2017.08.010

[40] J. Ereña, J. Vicente, A.T. Aguayo, A.G. Gayubo, M. Olazar, J. Bilbao, Effect of combining metallic and acid functions in CZA/HZSM-5 desilicated zeolite catalysts on the DME steam reforming in a fluidized bed, Int. J. Hydrogen Energy 38 (2013) 10019–10028. https://doi.org/10.1016/j.ijhydene.2013.05.134

[41] J. Bussi, M. Musso, S. Veiga, N. Bespalko, R. Faccio, A.-C. Roger, Ethanol steam reforming over NiLaZr and NiCuLaZr mixed metal oxide catalysts, Catal. Today 213 (2013) 42-49. https://doi.org/10.1016/j.cattod.2013.04.013

[42] A. Di Michele, A. Dell’Angelo, A. Tripodi, E. Bahadori, F. Sánchez, D. Motta, N. Dimitratos, I. Rossetti, G. Ramis, Steam reforming of ethanol over Ni/$MgAl_2O_4$ catalysts, Int. J. Hydrogen Energy 44 (2019) 952-964. https://doi.org/10.1016/j.ijhydene.2018.11.048

[43] H. Wang, Y. Liu, L. Wang, Y.N. Qin, Study on the carbon deposition in steam reforming of ethanol over Co/CeO_2 catalyst, Chem. Eng. J. 145 (2008) 25–31. https://doi.org/10.1016/j.cej.2008.02.021

[44] T.S. Moraes, R.C.R. Neto, M.C. Ribeiro, L.V. Mattos, M. Kourtelesis, X. Verykios, F.B. Noronha, Effects of ceria morphology on catalytic performance of Ni/CeO_2 catalysts for low temperature steam reforming of ethanol, Top. Catal. 58 (2015) 281–294. https://doi.org/10.1007/s11244-015-0369-x

[45] A. Ochoa, B. Aramburu, B. Valle, D.E. Resasco, J. Bilbao, A.G. Gayubo, P. Castaño, Role of oxygenates and effect of operating conditions in the deactivation of a Ni supported catalyst during the steam reforming of bio-oil, Green Chem. 19 (2017) 4315–4333.

[46] A. Ochoa, B. Aramburu, M. Ibáñez, B. Valle, J. Bilbao, A.G. Gayubo, P. Castaño, Compositional insights and valorization pathways for carbonaceous material deposited during bio-oil thermal treatment, ChemSusChem 7 (2014) 2597–2608. https://doi.org/10.1002/cssc.201402276

[47] B. Valle, B. Aramburu, M. Olazar, J. Bilbao, A.G. Gayubo, Steam reforming of raw bio-oil over Ni/La_2O_3-Al_2O_3: Influence of temperature on product yields and catalyst deactivation, Fuel 216 (2018) 463–474. https://doi.org/10.1016/j.fuel.2017.11.149

[48] A. Sadezky, H. Muckenhuber, H. Grothe, R. Niessner, U. Pöschl, Raman microspectroscopy of soot and related carbonaceous materials: Spectral analysis and structural information, Carbon 43 (2005) 1731–1742. https://doi.org/10.1016/j.carbon.2005.02.018

[49] J. Sourice, A. Quinsac, Y. Leconte, O. Sublemontier, W. Porcher, C. Haon, A. Bordes, E. De Vito, A. Boulineau, S. Jouanneau Si Larbi, N. Herlin-Boime, C. Reynaud, One-step synthesis of Si@C nanoparticles by laser pyrolysis: High-capacity anode material for lithium-ion batteries, ACS Appl. Mater. Interfaces 7 (2015) 6637–6644. https://doi.org/10.1021/am5089742

[50] A.G. Gayubo, A.T., Aguayo, A: Atutxa, B. Valle, J. Bilbao, Undesired components in the transformation of biomass pyrolysis-oil into hydrocarbons on a HZSM-5 zeolite, J. Chem. Technol. Biotechnol. 80 (2005) 1244-1251. https://doi.org/10.1002/jctb.1316

[51] M. Chen, Y. Wang, Z. Yang, T. Liang, S. Liu, Z. Zhou, X. Li, Effect of Mg-modified mesoporous Ni/Attapulgite catalysts on catalytic performance and resistance to carbon deposition for ethanol steam reforming, Fuel 220 (2018) 32-46. https://doi.org/10.1016/j.fuel.2018.02.013

FIGURE CAPTIONS

Figure 1. Evolution with time on stream of ethanol conversion and product yields at 500 ºC (a) and 650 ºC (b). Reaction conditions: space-time, 0.02 $g_{catalyst}h/g_{EtOH}$; S/E = 6.

Figure 2. Effect of temperature on the evolution with time on stream of ethanol conversion (a) and yields of H_2 (b), CO_2 (c), CO (d), CH_4 (e) and acetaldehyde (f). Reaction conditions: space-time, 0.18 $g_{catalyst}h/g_{EtOH}$; S/E = 3.

Figure 3. Effect of steam/ethanol ratio on the evolution with time on stream of ethanol conversion and H_2 yield (a), and yields of CO and CH_4 (b). Reaction conditions: 500 ºC; space-time, 0.18 $g_{catalyst}h/g_{EtOH}$.

Figure 4. Effect of space-time on the evolution with time on stream of ethanol conversion (a) and yields of H_2 (b), CO (c), CH_4 (d), acetaldehyde (e) and ethylene (f). Reaction conditions: 550 ºC; S/E = 6.

Figure 5. Effect of space-time on the TPO profiles of deactivated catalyst. Reaction conditions: Graph a: 500 ºC; S/E = 6; Graph b: 600 ºC; S/E = 3.

Figure 6. Effect of space-time on the coke content deposited for two values of S/E ratio at 500 ºC (a) and 600 ºC (b).

Figure 7. Effect of reaction temperature on the TPO profiles on deactivated catalyst. Reaction conditions: S/E = 6; space-time: 0.02 $g_{catalyst}h/g_{EtOH}$ (a) and 0.09 $g_{catalyst}h/g_{EtOH}$ (b).

Figure 8. Effect of steam/ethanol ratio on the TPO profiles of deactivated catalyst at 500 ºC (a) and 600 ºC (b). space-time, 0.18 $g_{catalyst}h/g_{EtOH}$.

Figure 9. SEM images of the coke deposited on the catalyst at 500 ºC, S/E=6 and space-time of 0.04 (a) and 0.18 $g_{catalyst}h/g_{EtOH}$ (b).

Figure 10. Raman spectra of the catalyst deactivated at two temperatures (a) and two values of S/E ratio (b). Reaction conditions: Graph a: space-time, 0.04 $g_{cat}h/g_{EtOH}$; S/E = 3. Graph b: 500 ºC; space-time, 0.35 $g_{catalyst}h/g_{EtOH}$.

Figure 11. Evolution with time on stream of ethanol conversion and product yields in a experiment of 200 h. Reaction conditions: 600 ºC; space time, 0.35 $g_{catalyst}h/g_{EtOH.}$; S/E = 3.

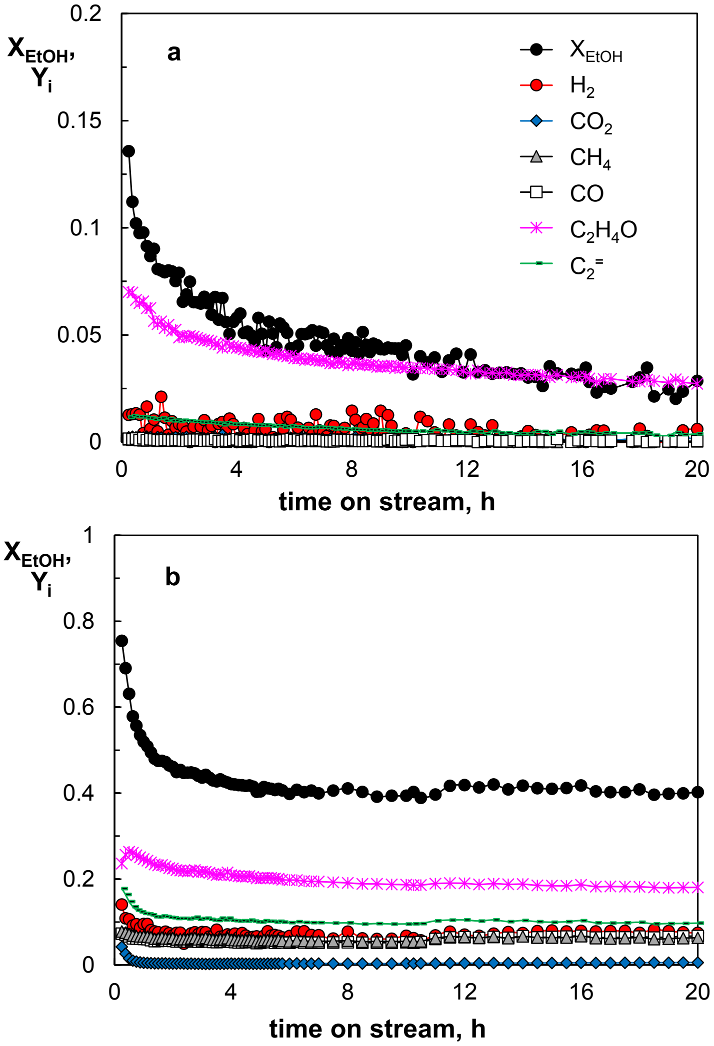
a
X_{EtOH}, Y_i
0.2
0.15
0.1
0.05
0
0
4
8
12
16
20
time on stream, h
X_{EtOH}
H_2
CO_2
CH_4
CO
C_2H_4O
$C_2^=$
b
X_{EtOH}, Y_i
1
0.8
0.6
0.4
0.2
0
0
4
8
12
16
20
time on stream, h

Figure 1

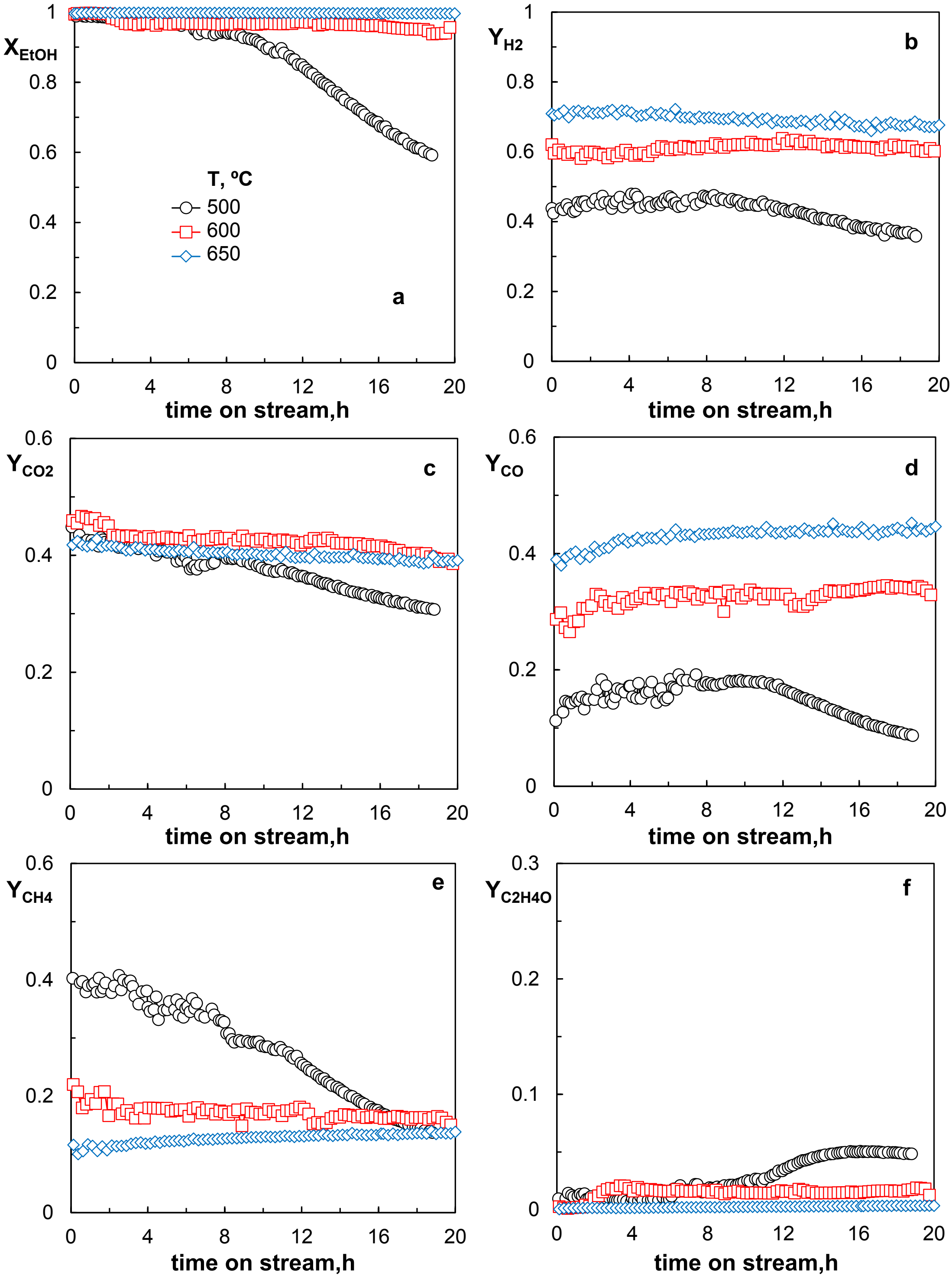

1
X_{EtOH}
0.8
0.6
0.4
0.2
0
T, ºC
500
600
650
a
0
4
8
12
16
20
time on stream,h
1
Y_{H2}
0.8
0.6
0.4
0.2
0
b
0
4
8
12
16
20
time on stream,h
0.6
Y_{CO2}
0.4
0.2
0
c
0
4
8
12
16
20
time on stream,h
0.6
Y_{CO}
0.4
0.2
0
d
0
4
8
12
16
20
time on stream,h
0.6
Y_{CH4}
0.4
0.2
0
e
0
4
8
12
16
20
time on stream,h
0.3
Y_{C2H4O}
0.2
0.1
0
f
0
4
8
12
16
20
time on stream,h

Figure 2

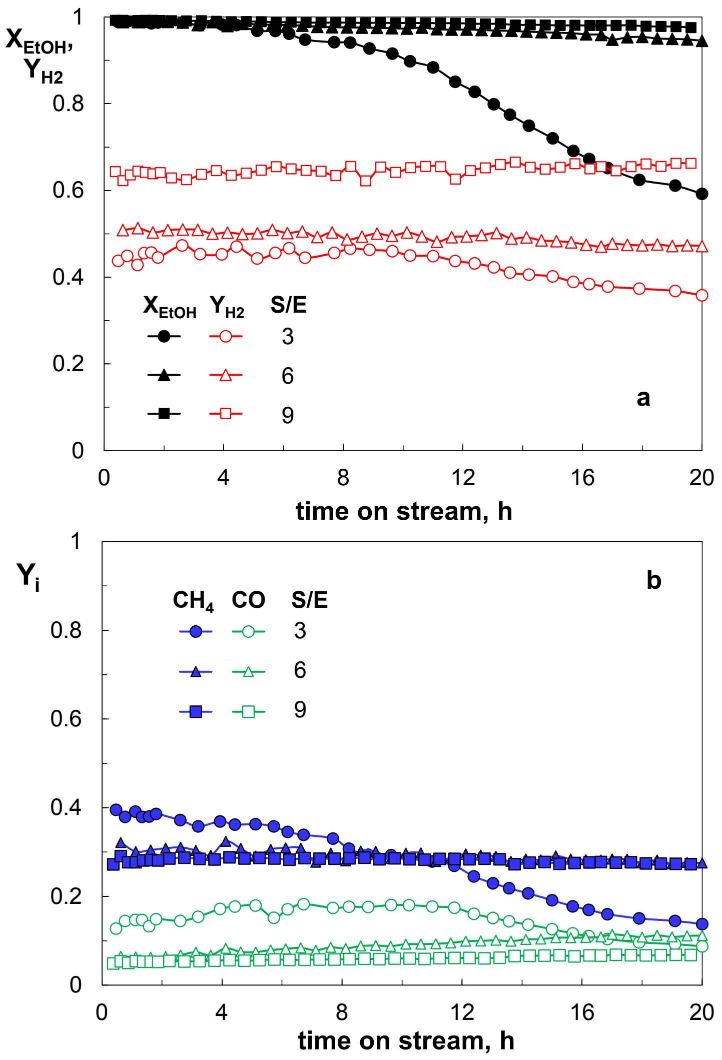
X_{EtOH}, Y_{H2}
1
0.8
0.6
0.4
0.2
0
X_{EtOH} Y_{H2} S/E
3
6
9
a
0
4
8
12
16
20
time on stream, h
Y_i
1
0.8
0.6
0.4
0.2
0
b
CH_4 CO S/E
3
6
9
0
4
8
12
16
20
time on stream, h

Figure 3

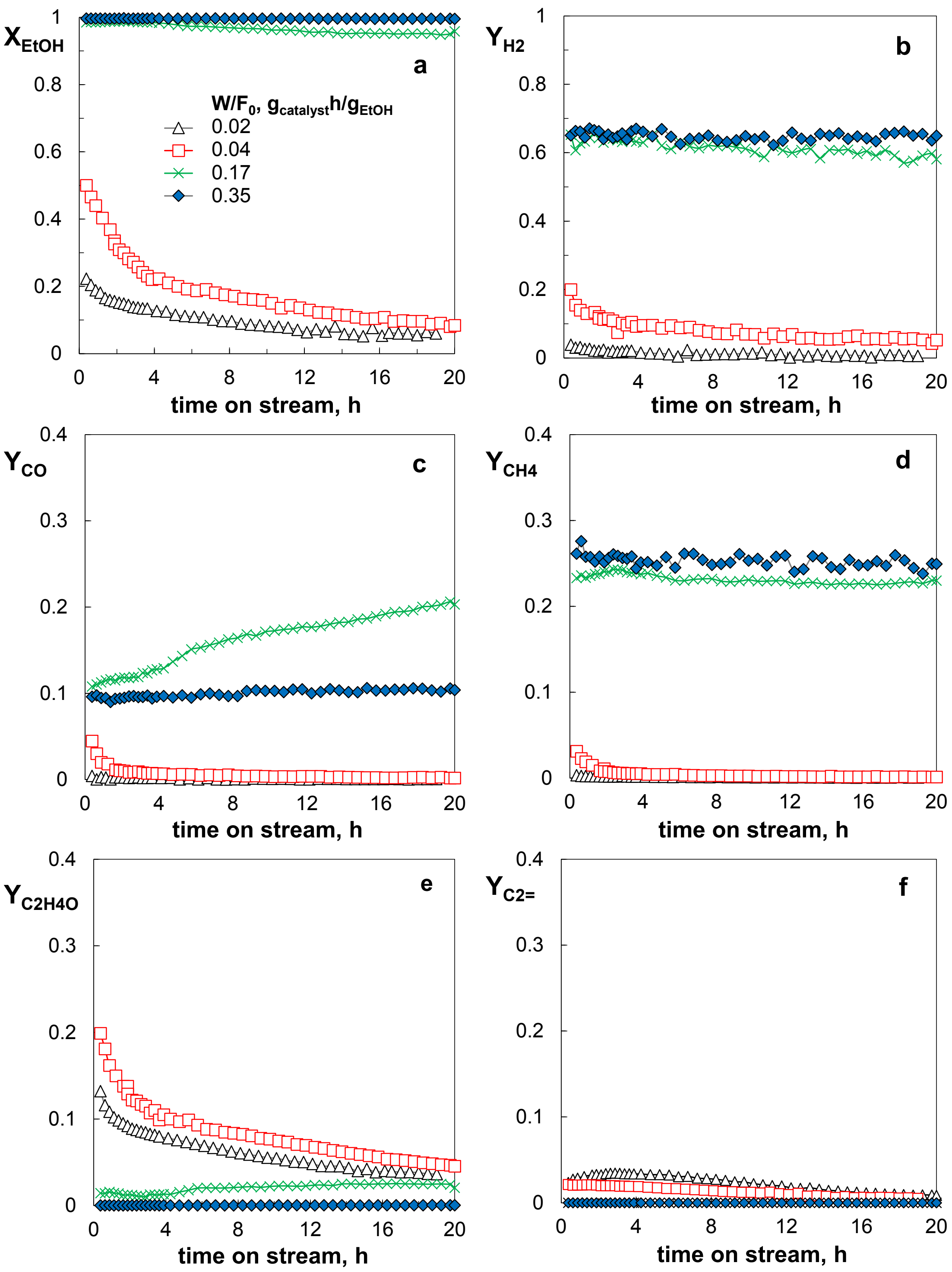
a
X_{EtOH}
1
0.8
0.6
0.4
0.2
0
W/F_0, $g_{catalyst}h/g_{EtOH}$
△ 0.02
□ 0.04
× 0.17
◆ 0.35
0
4
8
12
16
20
time on stream, h
b
Y_{H2}
1
0.8
0.6
0.4
0.2
0
time on stream, h
c
Y_{CO}
0.4
0.3
0.2
0.1
0
time on stream, h
d
Y_{CH4}
time on stream, h
e
Y_{C2H4O}
time on stream, h
f
$Y_{C2=}$
time on stream, h

Figure 4

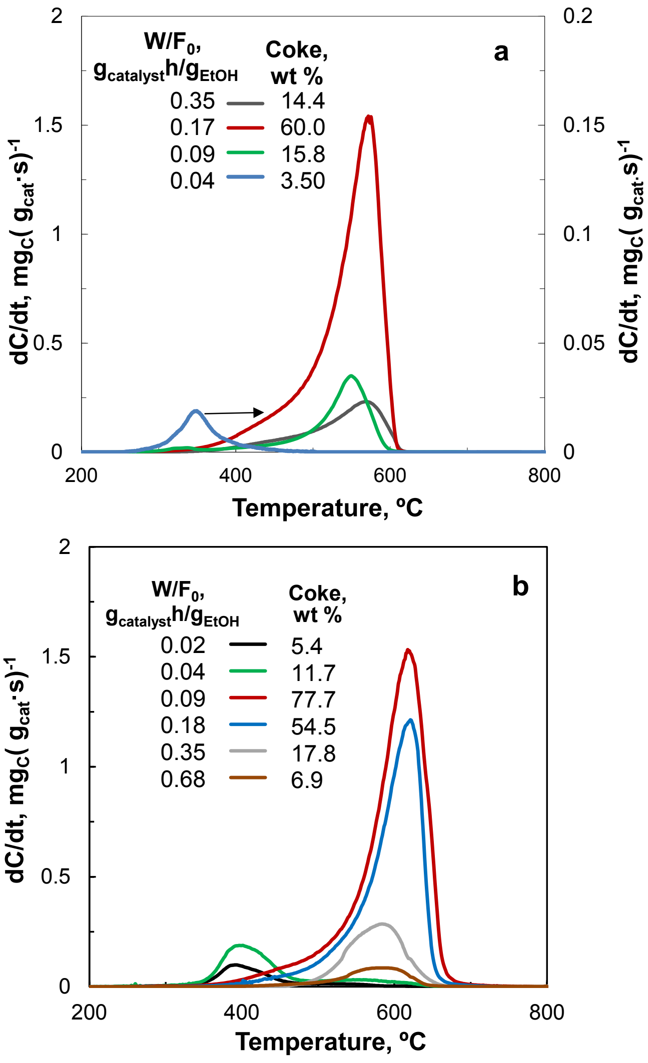
a
W/F$_0$, g$_{catalyst}$h/g$_{EtOH}$
Coke, wt %
0.35 14.4
0.17 60.0
0.09 15.8
0.04 3.50
dC/dt, mg$_C$(g$_{cat}$·s)$^{-1}$
0
0.5
1
1.5
2
0
0.05
0.1
0.15
0.2
200
400
600
800
Temperature, ºC
b
W/F$_0$, g$_{catalyst}$h/g$_{EtOH}$
Coke, wt %
0.02 5.4
0.04 11.7
0.09 77.7
0.18 54.5
0.35 17.8
0.68 6.9
dC/dt, mg$_C$(g$_{cat}$·s)$^{-1}$
0
0.5
1
1.5
2
200
400
600
800
Temperature, ºC

Figure 5

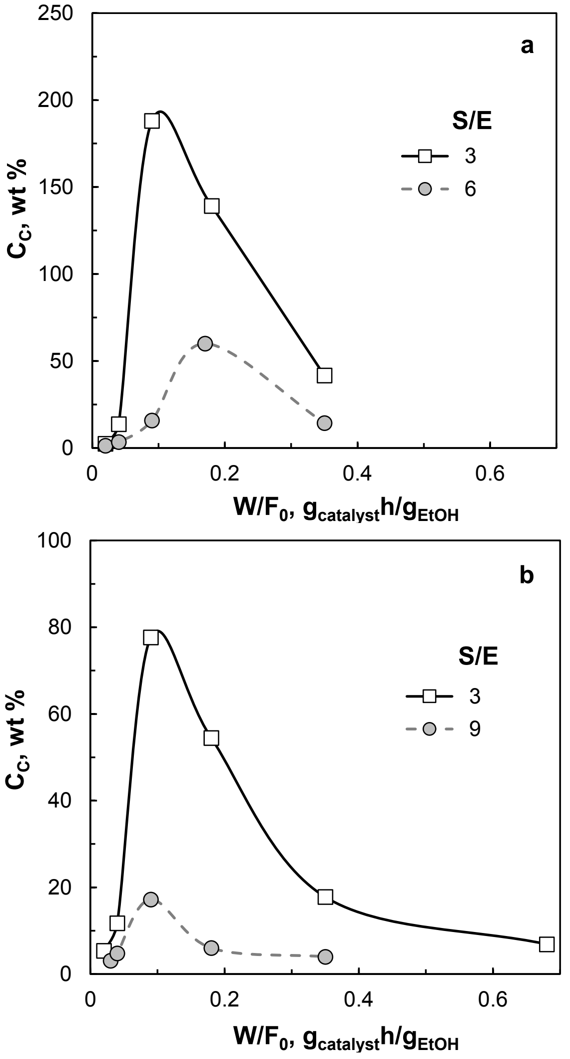
a
250
200
150
100
50
0
C_C, wt %
S/E
3
6
0
0.2
0.4
0.6
W/F_0, $g_{catalyst}$h/g_{EtOH}
b
100
80
60
40
20
0
C_C, wt %
S/E
3
9
0
0.2
0.4
0.6
W/F_0, $g_{catalyst}$h/g_{EtOH}

Figure 6

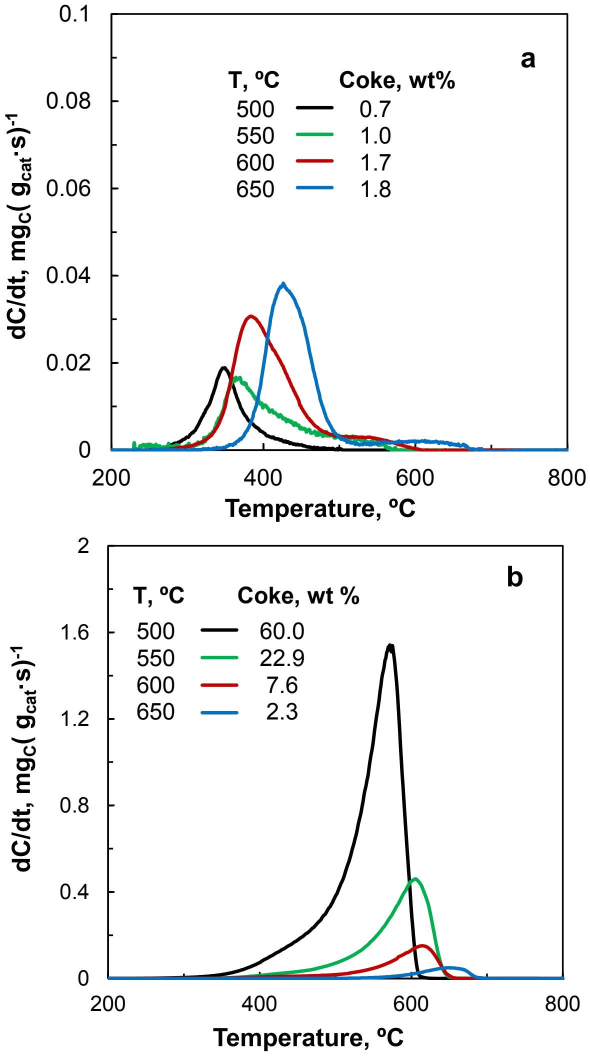
a
T, ºC
Coke, wt%
500
0.7
550
1.0
600
1.7
650
1.8
dC/dt, mg$_C$(g$_{cat}$·s)$^{-1}$
0.1
0.08
0.06
0.04
0.02
0
200
400
600
800
Temperature, ºC
b
T, ºC
Coke, wt %
500
60.0
550
22.9
600
7.6
650
2.3
dC/dt, mg$_C$(g$_{cat}$·s)$^{-1}$
2
1.6
1.2
0.8
0.4
0
200
400
600
800
Temperature, ºC

Figure 7

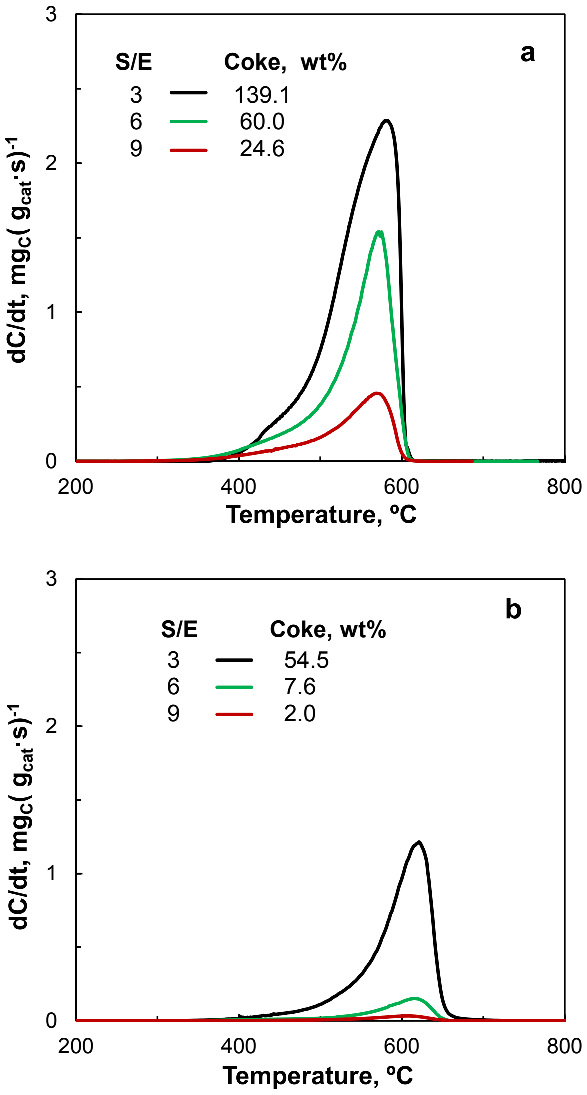
a
S/E
Coke, wt%
3
139.1
6
60.0
9
24.6
dC/dt, $mg_C(g_{cat} \cdot s)^{-1}$
0
1
2
3
200
400
600
800
Temperature, ºC
b
S/E
Coke, wt%
3
54.5
6
7.6
9
2.0
dC/dt, $mg_C(g_{cat} \cdot s)^{-1}$
0
1
2
3
200
400
600
800
Temperature, ºC

Figure 8

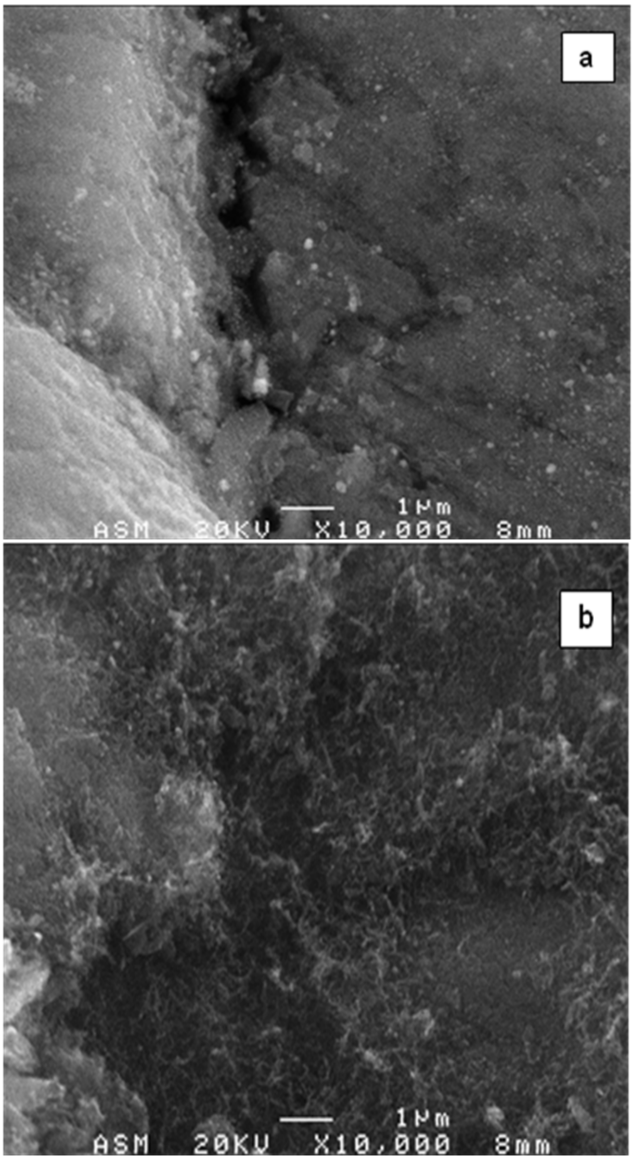

Figure 9

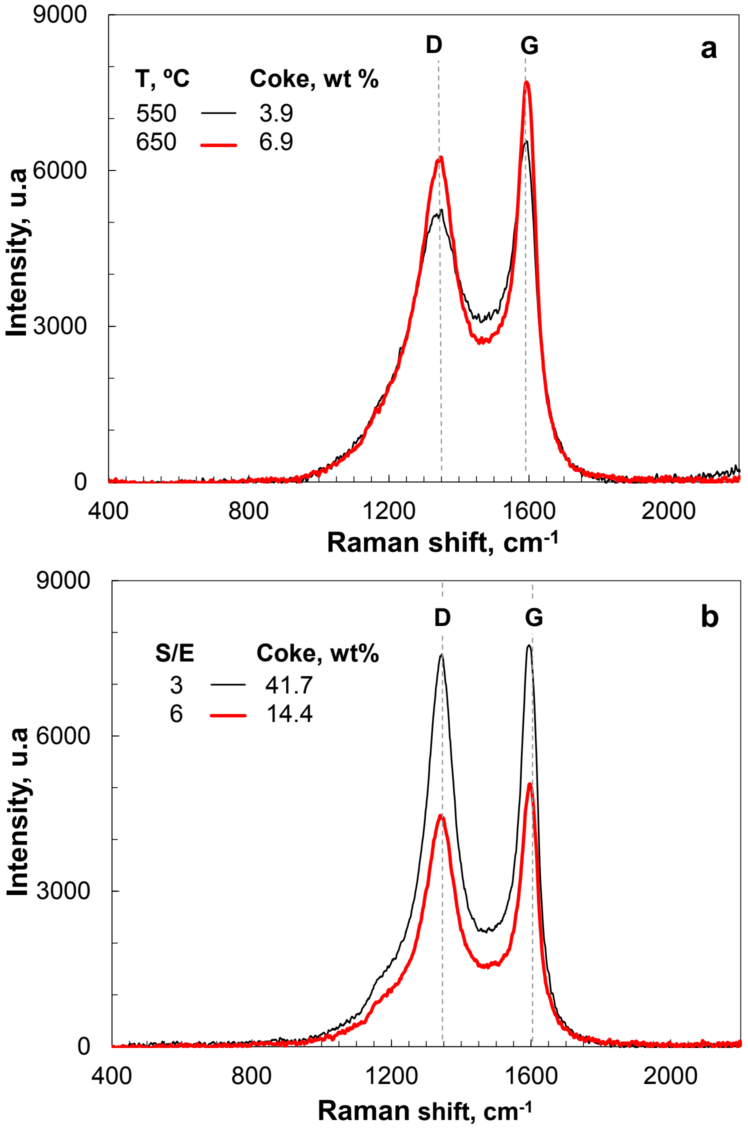
a
D
G
T, ºC
Coke, wt %
550
3.9
650
6.9
Intensity, u.a
9000
6000
3000
0
400
800
1200
1600
2000
Raman shift, cm-1
b
D
G
S/E
Coke, wt%
3
41.7
6
14.4
Intensity, u.a
9000
6000
3000
0
400
800
1200
1600
2000
Raman shift, cm-1

Figure 10

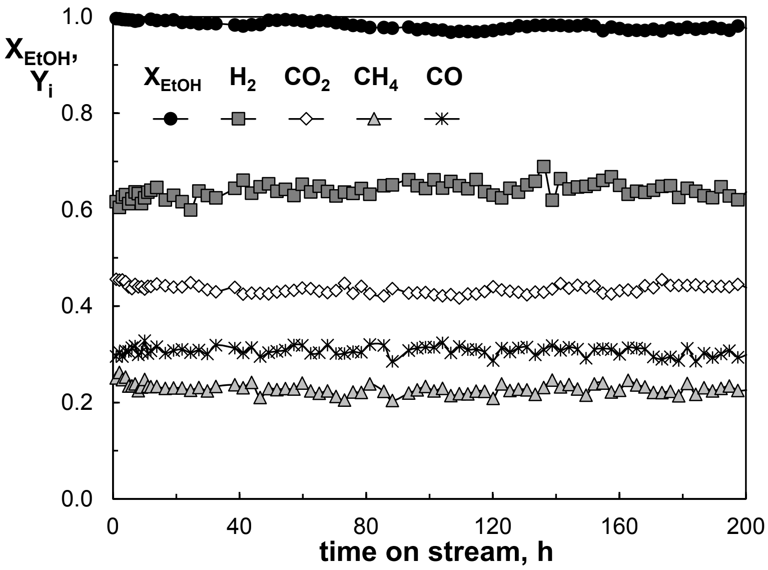
X_{EtOH}, Y_i
1.0
0.8
0.6
0.4
0.2
0.0
X_{EtOH}
H_2
CO_2
CH_4
CO
0
40
80
120
160
200
time on stream, h

Figure 11

Table 1. Secondary reactions of gaseous by-products formation and coke formation-gasification reactions in ethanol steam reforming.

Ethanol dehydrogenation	$C_2H_5OH \rightarrow C_2H_4O + H_2$	(2)
Ethanol dehydration	$C_2H_5OH \rightarrow C_2H_4 + H_2O$	(3)
Acetaldehyde decomposition	$C_2H_4O \rightarrow CO + CH_4$	(4)
Ethanol decomposition	$C_2H_5OH \rightarrow CO + CH_4 + H_2$	(5)
Water Gas Shift (WGS) reaction	$CO + H_2O \leftrightarrow CO_2 + H_2$	(6)
Methanation↔methane steam reforming	$CO + 3\ H_2 \leftrightarrow CH_4 + H_2O$	(7)
Ethylene steam reforming	$C_2H_4 + 2H_2O \rightarrow 2CO + 4H_2$	(8)
Coke formation/gasification reactions:		
Ethanol cracking:	$C_2H_5OH \rightarrow$ gases (H_2, CO, CO_2, CH_4) + Coke	(9)
Acetaldehyde cracking:	$C_2H_4O \rightarrow$ gases (H_2, CO, CO_2, CH_4) +Coke	(10)
Ethylene polymerization:	$C_2H_4 \rightarrow$ polymers $\rightarrow$ Coke	(11)
Methane decomposition:	$CH_4 \rightarrow 2H_2 + C$	(12)
Boudouard reaction:	$2CO \leftrightarrow C + CO_2$	(13)
Coke gasification:	Coke + $H_2O \rightarrow CO + H_2$	(14)

Table 2. Physical properties of the catalyst fresh and used with different space time values. Reaction conditions: 500 ºC, S/E = 6.

Catalyst	S_{BET}, m^2/g	V_{pore}, cm^3/g	d_{pore}, Å	**Coke content**, wt%
fresh	35.3	0.179	30.90	--
deactivated (0.04 $g_{catalyst}h/g_{EtOH}$)	35.1	0.198	30.95	3.5
deactivated (0.18 $g_{catalyst}h/g_{EtOH}$)	156.6	0.159	9.55	60.0

Table 3. Effect of reaction conditions of the Ni^0 crystal size for the catalyst deactivated in long duration runs (200 h).

Reaction conditions		d_{MO} (Ni^0), nm (regenerated catalyst) $2\theta = 52^o$	**Coke content**, wt%
T, ºC	**S/E**		
600	3	11	76
600	6	12	53
600	6	12	42

Table 4. Characteristic parameters of Raman spectra for the catalyst used with different reaction conditions.

Space time, $g_{catalyst}h/g_{EtOH}$	**T**, ºC	**S/E**	I_D/I_G	**G band** location, cm^{-1}	 width, cm^{-1}
0.04	550	3	2.31	1590.4	65.2
	650		1.94	1594.3	56.9
0.35	500	3	1.80	1594.3	52.2
		6	0.84	1595.2	51.5

SUPPORTING INFORMATION

Origin and nature of coke in ethanol steam reforming and its role in deactivation of Ni/La_2O_3-αAl_2O_3 catalyst

Carolina Montero[a*], *Aingeru Remiro*[b], *Lide Oar-Arteta*[b,c], *Beatriz Valle*[b], *Javier Bilbao*[b], *Ana G. Gayubo*[b]

[a] *Chemical Engineering Faculty, Central University of Ecuador, Ciudad Universitaria-Ritter s/n y Bolivia. Quito, Ecuador. Phone: +593 22544631. Fax: +593 22529676*

[b] *Chemical Engineering Department, University of the Basque Country, P.O. Box 644, 48080. Bilbao, Spain. Phone: +34 946 015361. Fax: +34 946 013 500*

[c]*TUDelft??*

*email: carodrmontero@gmail.com

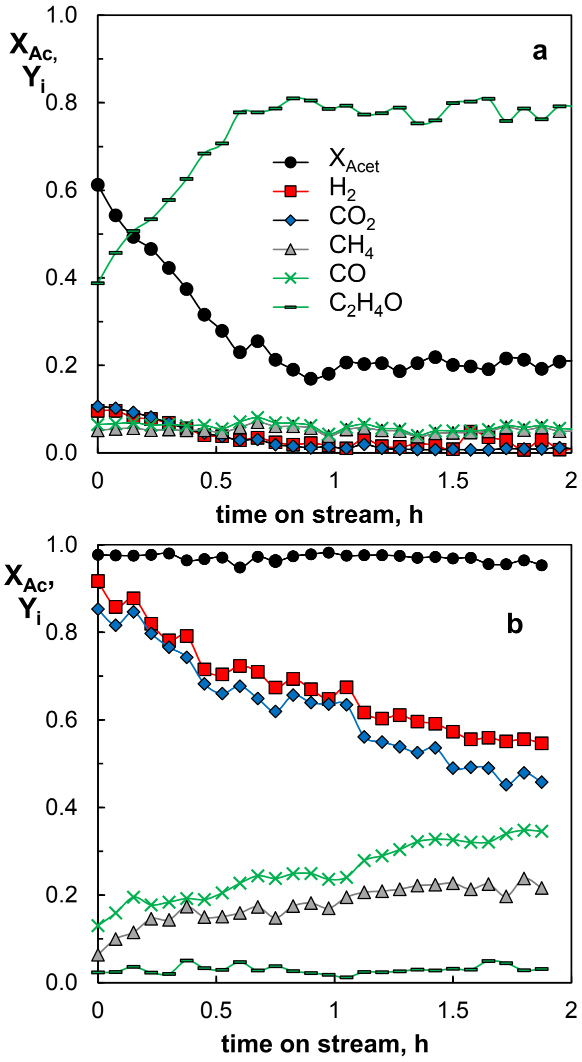

Figure S1. Evolution with time on stream S of conversion (X_{Ac}) and products yield (Y_i), in the SR of acetaldehyde. Reaction conditions: 600 ºC, S/Ac = 12; W/F$_0$ = 0.04 $g_{catalyst}h/g_{Ac}$ (a) and 0.21$g_{catalyst}h/g_{Ac}$ (b).

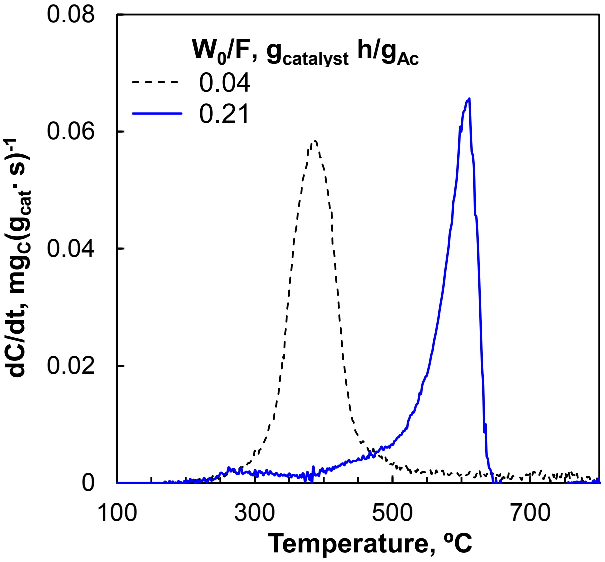

Figure S2. TPO profiles of the catalyst used in the SR of acetaldehyde with different space time values. Reaction conditions: 600 ºC, S/Ac=12, P_{Ac}=0.083 bar